PNAS RESEARCH ARTICLE | PHYSICS

Quantum oscillations in the magnetization and density of states of insulators

Animesh Panda[a], Sumilan Banerjee[a,1], and Mohit Randeria[b,1]

Edited by J. C. Davis, University of Oxford, Oxford, United Kingdom; received May 15, 2022; accepted August 22, 2022

The observation of $1/B$-periodic behavior in Kondo insulators and semiconductor quantum wells challenges the conventional wisdom that quantum oscillations (QOs) necessarily arise from Fermi surfaces in metals. We revisit recently proposed theories for this phenomenon, focusing on a minimal model of an insulator with a hybridization gap between two opposite-parity light and heavy mass bands with an inverted band structure. We show that there are characteristic differences between the QO frequencies in the magnetization and the low-energy density of states (LE-DOS) of these insulators, in marked contrast to metals where all observables exhibit oscillations at the same frequency. The magnetization oscillations arising from occupied Landau levels occur at the same frequency that would exist in the unhybridized case. The LE-DOS oscillations in a disorder-free system are dominated by gap-edge states and exhibit a beat pattern between two distinct frequencies at low temperature. Disorder-induced in-gap states lead to an additional contribution to the DOS at the unhybridized frequency. The temperature dependence of the amplitude and phase of the magnetization and DOS oscillations are also qualitatively different and show marked deviations from the Lifshitz–Kosevich form well known in metals. We also compute transport to ensure that we are probing a regime with insulating upturns in the direct current (DC) resistivity.

quantum oscillations | Kondo insulators | hybridization-gap insulator

Significance

The Fermi surface, the defining characteristic of metals, leads to oscillatory behavior as a function of the magnetic field in various experiments. It was thus a great surprise when such oscillations were recently seen in insulators without any Fermi surface. Here we develop a general theory of quantum oscillations in insulators. We find that, in striking contrast to metals, the oscillation frequency for magnetization differs from observables like the resistivity, which depend on the low-energy density of states of electronic excitations. To complement our detailed analysis of their frequency, phase, and temperature-dependent amplitude, we present a simple physical picture for understanding why quantum oscillations occur in insulators and why they differ in significant ways from the well-understood metallic case.

Metals are characterized by electronic excitations that are gapless on a locus in momentum space called the Fermi surface. The most direct probe of the Fermi surface is quantum oscillations (1) in various thermodynamic and transport measurements that are periodic in the inverse magnetic field. Insulators, on the other hand, are characterized by a gap, i.e., the absence of low-energy excitations that respond to electromagnetic fields. It thus came as a great surprise that Kondo insulators SmB_6 and YbB_{12} were found to exhibit $1/B$-periodic oscillations (2–6), despite the absence of gapless electronic excitations in the bulk. Quantum oscillations have now also been observed in InAs/GaSb semiconductor quantum wells (7, 8).

Soon after the first experiments, Knolle and Cooper (KC) (9) pointed out that a simple model of an insulator with a hybridization gap can exhibit deHass van Alphen (dHvA) oscillations in the magnetization even in the absence of a Fermi surface. The KC ideas have been extended to include more realistic band structure, hybridization (10, 11), and impurity states (12) with a focus on the low-energy density of states (LE-DOS) oscillations, which are a proxy for the Shubnikov deHass (SdH) oscillations in transport.

Kondo insulators are strongly correlated, and many exotic mechanisms (Majorana fermions, fractionalized phases, topological excitations, magnetoexcitons) (13–19) have also been proposed for understanding the observed oscillations. However, their observation in semiconductor quantum wells strongly suggests that this phenomenon is not restricted to correlated materials and is more general than previously anticipated.

In this paper we revisit the hybridization gap insulator (9, 10, 12, 20–26) motivated by the following question that has not been addressed in earlier work. What actually determines the frequency of quantum oscillations in an insulator, since—unlike metals—there is no Fermi surface whose extremal area is being probed? We find a surprising answer. In marked contrast to metals, different observables in hybridization gap insulators show different frequencies, for which we find analytical expressions and provide a simple physical semiclassical picture.

For a clean insulator without any disorder, we show that all occupied Landau levels contribute to the magnetization (dHvA) oscillations, whose frequency F_0 is governed by the area of the Fermi surface that would have existed in the absence of hybridization. On the other hand, the low-temperature SdH oscillations in the LE-DOS are dominated by gap-edge states and exhibit two distinct frequencies $F_0 \pm \delta F$ corresponding to the locus of the top (bottom) of the valence (conduction) band. We also show that the dHvA and SdH oscillations exhibit characteristic T-dependent amplitudes and field damping,

Author affiliations: [a]Centre for Condensed Matter Theory, Department of Physics, Indian Institute of Science, Bangalore 560012, India; and [b]Department of Physics, The Ohio State University, Columbus, OH 43210

Author contributions: S.B. and M.R. designed research; A.P., S.B., and M.R. performed research; and A.P., S.B., and M.R. wrote the paper.

The authors declare no competing interest.

This article is a PNAS Direct Submission.

[1]To whom correspondence may be addressed. Email: sumilan@iisc.ac.in or randeria.1@osu.edu.

This article contains supporting information online at https://www.pnas.org/lookup/suppl/doi:10.1073/pnas.2208373119/-/DCSupplemental.

Published October 10, 2022.

Table 1. Summary of results for the low-energy DOS and magnetization (M) oscillations in a hybridization-gap insulator with indirect gap $\Delta_I \gg$ impurity broadening

Observable	Contributing states	Frequency	Field dependence of amplitude	T dependence ($T \to 0$ limit)
LE-DOS	Gap-edge states	$F_0 \pm \delta F$	$\exp\left[-\frac{\pi\Delta_I T}{(\hbar\omega_c)^2}\right]$	Nonmonotonic [$\exp(-\Delta_I/2T)$]
	In-gap states (impurities)	F_0	$\exp\left(-\frac{\pi\Delta_I}{2\hbar\omega_c}\right)$	Monotonically decreasing (constant)
Magnetization M	All occupied states	F_0	$\exp\left(-\frac{\pi\Delta_I}{2\hbar\omega_c}\right)$	Nonmonotonic (constant)

$F_0 = (\hbar/2\pi e)\pi k_F^2$ is the unhybridized frequency, $\delta F = -(m_2 - m_1)\Delta_I/(4\hbar e)$, and the cyclotron frequency $\omega_c = eB/(m_1 + m_2)$, where k_F is the unhybridized crossing in $\boldsymbol{k}$ space between bands with masses m_1 and m_2. The "nonmonotonic" T dependence is qualitatively different from the LK result in metals, while the "monotonically decreasing" amplitude is of the LK form; see main text.

which differ from the standard Lifshitz–Kosevich (LK) results for metals (1). Our main results are summarized in Table 1.

Disorder induces in-gap states that impact the quantum oscillations in interesting ways. The dHvA frequency is unchanged, while the LE-DOS exhibits additional oscillations at F_0 along with those arising from the gap edges. Our results, for which we provide a simple physical picture, are obtained using analytical saddle-point calculations in the semiclassical regime, together with extensive numerical calculations, and give insight into the frequency, phase, and amplitude of the quantum oscillations and their dependence on temperature, magnetic field, and disorder.

We introduce in *Section 2* our minimal model of a hybridization gap insulator and describe its Landau-level spectrum (Fig. 1). In *Section 3* we explain the physical origin of the differences between the dHvA and SdH oscillations in an insulator, which are summarized in Fig. 2. Our analytical and numerical results for the low-energy DOS are described in *Section 4* and the results for magnetization in *Section 5*. We conclude in *Section 6* with a brief discussion of quantum oscillation experiments in Kondo insulators and semiconductor quantum wells.

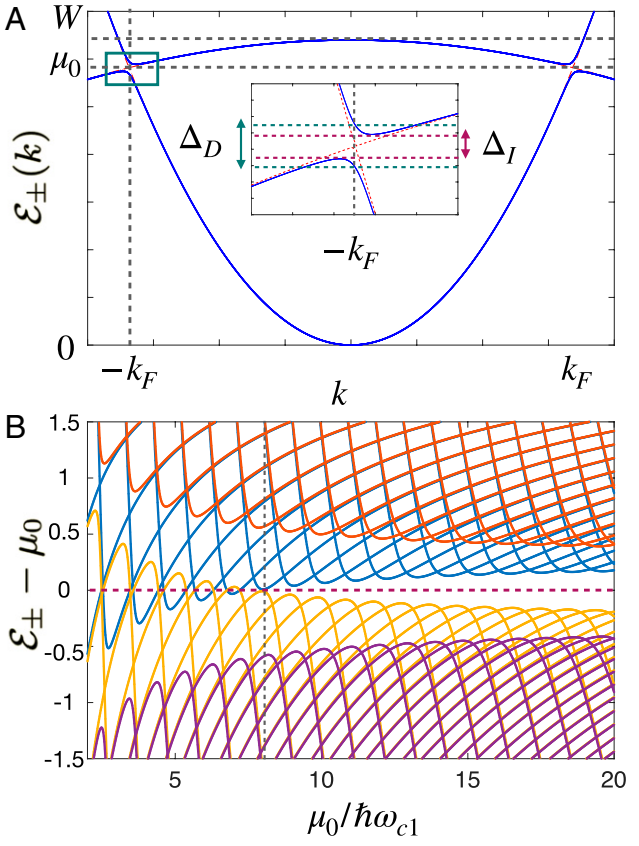

Fig. 1. Band structure and Landau levels. (*A*) Energy dispersion $\mathcal{E}_\pm(k)$ in the absence of disorder. *Inset* shows the indirect (Δ_I) and direct (Δ_D) gaps. (*B*) Energy levels $\mathcal{E}_{lb\pm}$ (Eq. **2**) for different LL indexes plotted as a function of $\mu_0/\hbar\omega_{c1} \propto 1/B$. We focus here on the regime $B < B_c$, the critical field (vertical dashed line) above which the system undergoes a field-induced insulator to metal transition; see main text and *SI Appendix*, section 3 for details. Energy is given in units of Δ_D. For our numerical calculations we use $m_2/m_1 = 10$ and $\Delta_D \approx 0.04W$.

1. Model

We consider a two-dimensional (2D) model of an insulator with two opposite-parity bands, a light "d" band and an inverted heavy "f " band (Fig. 1*A*), with p-wave hybridization. The Hamiltonian $\mathcal{H} = \sum_{\boldsymbol{k}} (d_{\boldsymbol{k}}^\dagger \;\; f_{\boldsymbol{k}}^\dagger) H_0(\boldsymbol{k}) (d_{\boldsymbol{k}} \;\; f_{\boldsymbol{k}})^T$ is given by

$$H_0(\boldsymbol{k}) = \begin{bmatrix} \epsilon_1(\boldsymbol{k})\mathbb{1} & v\boldsymbol{k}\cdot\boldsymbol{\sigma} \\ v\boldsymbol{k}\cdot\boldsymbol{\sigma} & \epsilon_2(\boldsymbol{k})\mathbb{1} \end{bmatrix}, \qquad [1]$$

Here $\boldsymbol{k} = (k_x, k_y)$, $\boldsymbol{\sigma} = (\sigma_x, \sigma_y)$ are Pauli matrices and $\mathbb{1}$ is the identity matrix in the spin space for the electron operators $d_{\boldsymbol{k}} = (d_{\boldsymbol{k}\uparrow} \;\; d_{\boldsymbol{k}\downarrow})^T$ and $f_{\boldsymbol{k}} = (f_{\boldsymbol{k}\uparrow} \;\; f_{\boldsymbol{k}\downarrow})^T$. The dispersion of the unhybridized bands is $\epsilon_1(\boldsymbol{k}) = \hbar^2 k^2/2m_1$ and $\epsilon_2(\boldsymbol{k}) = W - \hbar^2 k^2/2m_2$. Unless otherwise mentioned, we set the chemical potential μ at $\mu_0 = Wm_+/m_1$, corresponding to the crossing of the unhybridized bands. Here $m_\pm = m_1 m_2/(m_2 \pm m_1)$, and the Fermi wave vector $k_F = \sqrt{2m_+ W}/\hbar$.

The parameter v, which couples opposite spins in the two bands, controls the hybridization gap. As shown in Fig. 1*A*, the insulator has a direct band gap $\Delta_D = 2\sqrt{2m_+ W}\, v/\hbar$ and an indirect band gap $\Delta_I = 2[\sqrt{m_1 m_2}/(m_1 + m_2)]\Delta_D$. We choose v so that $\Delta_D \ll \mu_0$, so that the hierarchy of energy scales is $m_+ v^2/\hbar^2 \ll \Delta_I < \Delta_D \ll \mu_0 < W$. A table of symbols used in our analysis is given in *SI Appendix*, section 1 for ready reference.

The minimal model of Eq. **1**. has been widely used to study electronic properties (27) and quantum oscillations (10, 12) in Kondo insulators. It also has close similarity with models of InAs/GaSb quantum wells (7, 8, 11).

We incorporate the effects of impurities, following ref. 12, with an effective non-Hermitian Hamiltonian $H(\boldsymbol{k})$ obtained by replacing $\epsilon_j(\boldsymbol{k}) \to \epsilon_j(\boldsymbol{k}) - \imath\Gamma_j$ for bands $j = 1, 2$ in Eq. **1**. The frequency- and momentum-independent imaginary self-energies are impurity scattering rates $\Gamma_1, \Gamma_2 \geq 0$ for the light- and heavy-mass bands, respectively. For our numerical calculations we consider both $\Gamma_1 \geq \Gamma_2$ and $\Gamma_1 < \Gamma_2$. The ratio of the light- and heavy-band scattering rates is not important for any of our main conclusions and analytical derivations.

$H(\boldsymbol{k})$ can be diagonalized to obtain complex eigenvalues $\mathcal{E}_\pm(k) = (\epsilon_1 + \epsilon_2 - \imath\Gamma \pm \sqrt{(\epsilon_1 - \epsilon_2 - \imath\gamma)^2 + 4v^2k^2})/2$, where $\Gamma = \Gamma_1 + \Gamma_2$ and $\gamma = \Gamma_1 - \Gamma_2$. Each eigenvalue is twofold degenerate given the $\uparrow\downarrow$ and $\downarrow\uparrow$ hybridization.

Disorder leads to a finite DOS at the chemical potential. We focus here on the insulating regime ($|\gamma| < \Delta_D$) with a finite

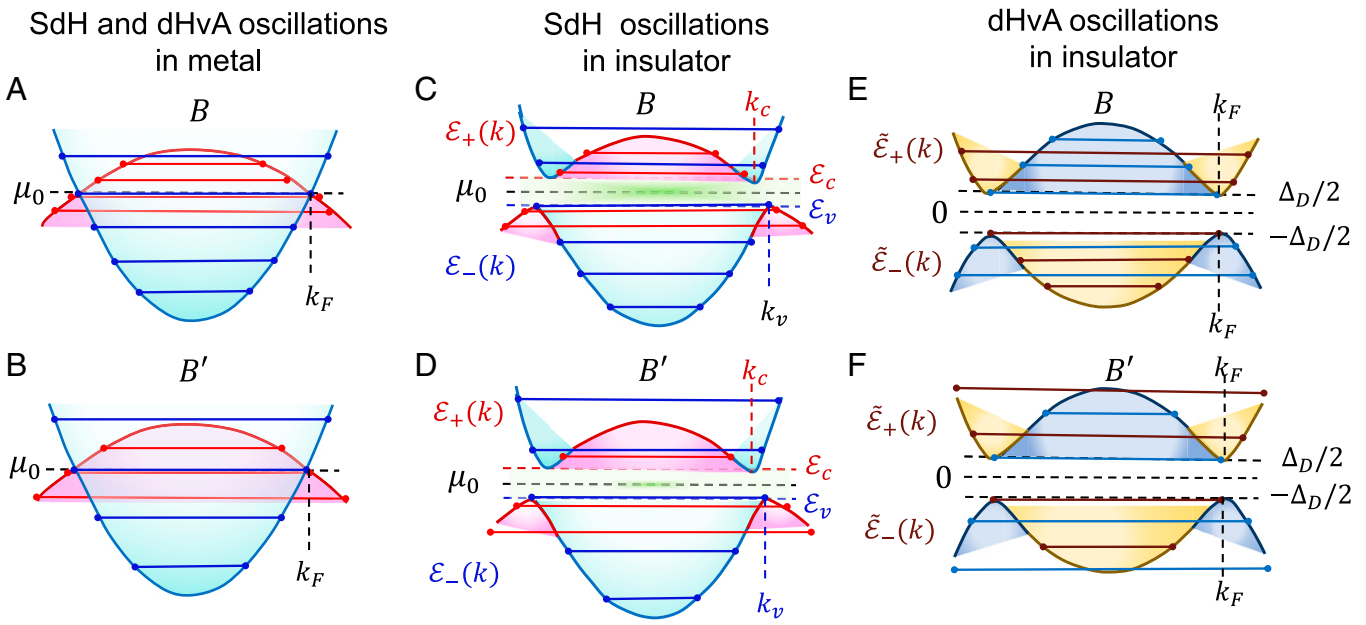

Fig. 2. Physical origin of the distinct frequencies for LE-DOS and magnetization oscillations. (*A* and *B*) Band structure and Landau levels in the limit of zero hybridization $v = 0$. For chemical potential at the band crossing energy $\mu_0 = \hbar^2 k_F^2/2m_1$ at the wavevector k_F, the SdH and dHvA oscillations have the same frequency F_0 determined by the Fermi surface area πk_F^2. The fields B and B' ($B < B'$) correspond to two successive crossings of an LL through μ_0. (*C* and *D*) At finite hybridization $v \neq 0$, the LE-DOS or SdH oscillations arise through thermal activation from crossing of energy levels through the hybridization-gap edges $\mathcal{E}_c$ and $\mathcal{E}_v$ of the conduction [$\mathcal{E}_+(k)$] and valence [$\mathcal{E}_-(k)$] bands, respectively. The areas πk_c^2 and πk_v^2 at the gap edges determine the frequencies. In addition, in the presence of disorder, the impurity-induced in-gap DOS (green shaded) has $1/B$-periodic modulation with frequency F_0. (*E* and *F*) The dHvA oscillations in magnetization arise from a *fictitious* particle-hole symmetric band structure $\tilde{\mathcal{E}}_\pm(k)$ centered around zero energy. At $T = 0$, the oscillations occur due to sequential entries or exits of additional energy levels, e.g., at fields B and B', into the electron-like part (yellow shaded) of $\mathcal{E}_-(k)$ from the hole-like part (blue shaded) of the band through the gap edge at $-\Delta_D/2$. The latter corresponds to the semiclassical orbit at wavevector k_F with area πk_F^2 and thus the frequency F_0 of dHvA oscillations in the hybridization-gap insulator.

gap $\mathrm{Re}[\mathcal{E}_+(k_F) - \mathcal{E}_-(k_F)] = \sqrt{\Delta_D^2 - \gamma^2}$ at k_F (12). We do not discuss the semimetallic regime ($|\gamma| \geq \Delta_D$) with zero gap, which exhibits usual (metallic) quantum oscillations.

The effect of Landau quantization in the presence of a magnetic field $\mathbf{B} = B\hat{\mathbf{z}}$ in the Hamiltonian $H(\boldsymbol{k})$ breaks the degeneracy of the eigenvalues for the $\uparrow\downarrow$ and $\downarrow\uparrow$ combinations, and we get four eigenvalues

$$\mathcal{E}_{l,b\pm} = \frac{\epsilon_{1,\ell_b} + \epsilon_{2,\ell_b'} - i\Gamma \pm \sqrt{(\epsilon_{1,\ell_b} - \epsilon_{2,\ell_b'} - i\gamma)^2 + \frac{8lv^2eB}{\hbar}}}{2}. \quad [2]$$

Here the Landau-level (LL) index $l \geq 1$ with $\ell_b = l, \ell_b' = l-1$ for $b = \uparrow\downarrow$, and $\ell_b = l-1, \ell_b' = l$ for $b = \downarrow\uparrow$ hybridizations. The $\pm$ signs refer to antibonding/bonding bands. $\epsilon_{1,l} = \hbar\omega_{c1}(l + 1/2)$ and $\epsilon_{2,l} = W - \hbar\omega_{c2}(l + 1/2)$ are LL energies for the unhybridized bands with cyclotron frequencies $\omega_{c1} = eB/m_1$ and $\omega_{c2} = eB/m_2$. The $l = 0$ LLs remain unchanged with energies $\epsilon_{1,0}$ and $\epsilon_{2,0}$ even for nonzero hybridization, but these are not relevant for the semiclassical limit $\mu_0/\hbar\omega_{c1} \gg 1$ that we focus on.

In the semiclassical limit $\ell' \approx \ell = l$ and $8lv^2eB/\hbar \approx 8l_F v^2 eB/\hbar = \Delta_D^2$ (with $l_F \simeq \mu_0/\hbar\omega_{c1}$) in Eq. **2** for Δ_D, Γ, $\gamma \ll \mu_0$ and energies near μ_0; see *SI Appendix*, section 2. Thus Eq. **2** reduces to the two doubly degenerate eigenvalues,

$$\mathcal{E}_{l\pm} = \left[\epsilon_{1,l} + \epsilon_{2,l} - i\Gamma \pm \sqrt{(\epsilon_{1,l} - \epsilon_{2,l} - i\gamma)^2 + \Delta_D^2}\right]/2. \quad [3]$$

The above LLs correspond to the k-space energy dispersion

$$\mathcal{E}_\pm(k) = \left[\epsilon_1 + \epsilon_2 - i\Gamma \pm \sqrt{(\epsilon_1 - \epsilon_2 - i\gamma)^2 + \Delta_D^2}\right]/2. \quad [4]$$

We use Eqs. **3** and **4** for our analytical calculations and to construct a simple physical picture of the SdH and dHvA oscillations in the insulator. We note that, in the absence of impurity scattering, our model has a field-induced transition from a gapped insulator to an gapless metal above a critical field $B_c = \sqrt{m_1 m_2}\Delta_D/e\hbar$ (*SI Appendix*, section 3). This can also be seen in Fig. 1*B*. We focus on the insulating regime $B < B_c$ in this paper.

2. Physical Picture of Quantum Oscillations in Insulators

Before turning to the details of our calculations, we present a physical picture to see why the LE-DOS (SdH) and magnetization (dHvA) oscillations in a hybridization-gap insulator differ from each other and why these results are so different from standard quantum oscillations in metals.

First, consider the limit of zero hybridization ($v = 0$) in the disorder-free Hamiltonian of Eq. **1**, which is a metal with overlapping electron and hole bands that cross at k_F at an energy μ_0 (Fig. 2 *A* and *B*). Both the bands give rise to SdH and dHvA oscillations with same frequency $F_0 = (\hbar/2\pi e)\pi k_F^2$ corresponding to the area of the semiclassical orbit at $\mu_0 = \hbar^2 k_F^2/2m_1$. LE-DOS oscillations arise due to the $1/B$-periodic passing of LLs across the chemical potential $\mu = \mu_0$. This occurs whenever ϵ_l matches μ and leads to SdH oscillations at frequency F_0. Each time a LL passes through μ, the total number of occupied LLs has a discrete jump leading to sharp periodic changes of the total energy $E(B) = N_B \sum_{\epsilon_l \leq \mu}(\epsilon_l - \mu)$, where $N_B = eB/h$ is the LL degeneracy. As a result, the $T = 0$ magnetization $M = -(\partial E/\partial B)$ oscillates as a function of $1/B$ with the same frequency F_0.

Next, consider the LE-DOS oscillations in the hybridization-gap insulator, focusing first on the disorder-free case, with the chemical potential μ_0 in the gap at the crossing of the

unhybridized bands (Fig. 2 *C* and *D*). The conduction-band edge $\mathcal{E}_c = \min \mathcal{E}_+(k)$ occurs at $k = k_c$, and the valence-band edge $\mathcal{E}_v = \max \mathcal{E}_-(k)$ at $k = k_v$, with $\mathcal{E}_{c/v} = \mu_0 \pm \Delta_I/2$. The LE-DOS oscillations arise from $1/B$-periodic passage of LLs through the conduction- and valence-band gap edges. In Fig. 2*C* it is at a field B and in Fig. 2*D* at higher field B' corresponding to successive crossing of a LL through band edges; i.e., $\mathcal{E}_{l+1,\pm}(B) = \mathcal{E}_{c/v}$ and $\mathcal{E}_{l\pm}(B) = \mathcal{E}_{c/v}$. This immediately leads to a $1/B$-periodic modulation of the DOS with frequencies $F_\pm$ determined by k_c and k_v of the gap-edge states, distinct from F_0 corresponding to the unhybridized k_F. We show below in *Section 4* (and *SI Appendix*, section 4) the SdH oscillations have frequencies $F_\pm = F_0 \mp (m_2 - m_1)\Delta_I/(4\hbar e)$. Clearly these oscillations need thermal excitation to the gap edge, which thus leads to an $\exp(-\Delta_I/2T)$ factor in the amplitude. What is less obvious is a field-damping (Dingle) factor of $\exp(-\pi\Delta_I T/(\hbar\omega_c)^2)$ that we find in our analysis below.

Impurities lead to in-gap spectral weight (12) at μ_0 that leads to oscillations at the unhybridized F_0 with an LK-like T dependence. We show below (using a semiclassical saddle-point analysis) that the LE-DOS oscillation is the sum of three pieces, the band-edge oscillations at $F_0 \pm \delta F$ and the impurity-induced oscillations at F_0, each with their characteristic T dependence and Dingle factors.

Finally, let us turn to the magnetization oscillations in the disorder-free insulator, which have a very different origin from that of the LE-DOS oscillations described above. The total energy $E(B) = N_B \sum_l (\mathcal{E}_{l-} - \mu)$ is given by a sum over all occupied states $\mathcal{E}_{l-}$ below the chemical potential μ, which is inside the gap. We next show that there is an unusual aspect (*SI Appendix*, section 8.A) to this sum that can be best seen by splitting $\mathcal{E}_{l-}$ into $\mathcal{E}_{l-} = \overline{\mathcal{E}}_{l-} + \widetilde{\mathcal{E}}_{l-}$ with $\overline{\mathcal{E}}_{l-} = (W + \hbar eBl/m_-)/2$ and $\widetilde{\mathcal{E}}_{l-} = -[(W - \hbar eBl/m_+)^2 + \Delta_D^2]^{1/2}/2$. This decomposition leads to $E(B) = E_{\rm nosc} + E_{\rm osc}$. It is easy to verify that $E_{\rm nosc} = \sum_l [\overline{\mathcal{E}}_{l-} - \mu]$ is a smooth monotonic function of B and the oscillations arise entirely from $E_{\rm osc} = \sum_l \tilde{\mathcal{E}}_{l-}$.

Thus the dHvA oscillations can be thought to arise from the valence band of a "fictitious" particle-hole symmetric band structure $\widetilde{\mathcal{E}}_\pm(k) = \pm[(W - \hbar^2k^2/2m_+)^2 + \Delta_D^2]^{1/2}/2$. Landau quantization of $\widetilde{\mathcal{E}}_\pm(k)$ leads to energy levels $\widetilde{\mathcal{E}}_{l\pm}$ for $B \neq 0$ shown in Fig. 2 *E* and *F*. The total energy $E(B)$ changes abruptly as the energy level $\widetilde{\mathcal{E}}_{l-}$ periodically enters the electron-like part of the fictitious valence band from the hole-like part through the gap edge (maximum) $\widetilde{\mathcal{E}}_v = -\Delta_D/2$ for some l and B. This occurs when $\widetilde{\mathcal{E}}_{l-} = \widetilde{\mathcal{E}}_v$, or equivalently $\hbar eBl/m_+ = W$, which leads to dHvA oscillations with unhybridized frequency F_0. This frequency corresponds to the semiclassical orbit of area πk_F^2 originating from the gap edge of the fictitious energy dispersion $\tilde{\mathcal{E}}_-(k)$. Remarkably, the actual chemical potential μ plays no role here and enters only the nonoscillatory part $E_{\rm nosc}$ as long as it lies in the gap.

We note that the same argument also gives a simple understanding of the dHvA oscillations in the original KC model (9) where one of the bands has infinite mass. The energy eigenvalues of the KC model can be obtained as the limiting case of Eq. **3** for $m_2 \to \infty$ and $\Gamma = 0$.

Does the unusual dichotomy between the SdH and dHvA oscillations that requires two different semiclassical orbit pictures (Fig. 2 *C*–*F*) indicate the failure of Onsager's rule of semiclassical area quantization for the hybridization-gap insulator? This is a crucial question, since in the general case of a nonparabolic dispersion the LL energy eigenvalues for the full quantum Hamiltonian in a field are not available and we must rely on Onsager's rule to deduce the quantum oscillation (QO) frequency. To answer this question, we explicitly verify Onsager's rule in our case by applying it to the energy dispersion $\mathcal{E}_\pm(k)$ of Eq. **4**. The dispersion is isotropic and thus the allowed k-space orbits in a B field are circles with quantized area $\pi k_l^2 = 2\pi leB/\hbar$ corresponding to semiclassical energy eigenvalues $\mathcal{E}_\pm(k_l)$. This exactly matches the LL energies of Eq. **4** obtained from our full quantum treatment. Thus, we will get the correct frequencies for SdH and dHvA oscillations and encounter the same dichotomy between them if the energy eigenvalues from Onsager's prescription are inserted into the expressions of LE-DOS and magnetization. In this sense, there is no violation of the semiclassical quantization rule for the hybridization-gap insulator. What is different from the standard theory, however, is that different parts of these energy eigenvalues contribute to the QOs in the LE-DOS and magnetization, This, as discussed above and shown in Fig. 2 *C*–*F*, leads to different effective semiclassical orbit pictures for dHvA and SdH oscillations. Hence, a "universal" semiclassical picture that applies to all physical quantities, like in a metal, does not work in hybridization-gap insulators.

3. Low-Energy DOS

In this section we discuss the oscillations in LE-DOS, a proxy for SdH oscillations, defined as

$$D(T) = -\int_{-\infty}^{\infty} d\xi \frac{\partial n_{\rm F}(\xi, T)}{\partial \xi} A(\xi). \qquad [5]$$

The Fermi function $n_{\rm F}(\xi, T) = (e^{\beta\xi} + 1)^{-1}$ with $\beta = 1/T$ ($k_{\rm B} = 1$), and the single-particle DOS (per unit area)

$$A(\xi) = -\left(\frac{N_B}{\pi}\right) {\rm Im} \sum_{l,b,p=\pm} \frac{1}{\xi + \mu_0 - \mathcal{E}_{l,bp}} \qquad [6]$$

is obtained from the complex eigenvalues of Eq. **2**, and $N_B = Be/h$ is the LL degeneracy.

We focus only on the oscillatory part of DOS and LE-DOS, and to make analytical progress, we convert the LL sum in Eq. **6** into an integral using the Poisson summation formula. In the limit $\mu_0 \gg \hbar\omega_{c1}$ using the semiclassical approximation $\mathcal{E}_{l,b\pm} \approx \mathcal{E}_{l\pm}$ (Eq. **3**) we obtain

$$A(\xi) = \frac{1}{2\pi^2\hbar^2} {\rm Im} \sum_{p=\pm, k\neq 0} \int_{l=0^-}^{\infty} dl\, e^{2\pi\imath kl} \frac{c_p(\xi)}{l - l_p(\xi)}. \qquad [7]$$

The integer k labels harmonics, and $l_p(\xi)$ and $c_p(\xi)$ are the poles and residues of $(\xi + \mu_0 - \mathcal{E}_{lp})^{-1}$ in the complex l plane (*SI Appendix*, section 5).

For $\mu_0 \gg \hbar\omega_{c1}$, we can extend the lower limit of the integral to $-\infty$ since ${\rm Re}(l_\pm) \gg 1$ and the poles are far from the origin. The oscillatory part (12) of the DOS is thus

$$A(\xi) = \frac{1}{\pi\hbar^2} {\rm Im} \sum_{k\neq 0, p=\pm} i s_p(\xi) c_p(\xi) e^{2\pi\imath k s_p(\xi) l_p(\xi)}, \qquad [8]$$

with $s_p = {\rm sgn}[{\rm Im}(l_p)]$. Substituting this in Eq. **5**, we obtain the oscillatory part of $D(T)$ by evaluating the energy integral as follows (see *SI Appendix*, section 6 for details):

At low temperature $T \ll \Delta_I$, the main contribution comes from two saddle points in the complex ξ-plane $\widetilde{\xi}_{k\pm} \simeq -\imath\Gamma_c \pm \Delta_I/2 + \mathcal{O}(k^2T^2/\hbar^2\omega_c^2)$, where $\omega_c = eB/(m_1 + m_2)$ and

$\Gamma_c = (m_1\Gamma_1 + m_2\Gamma_2)/(m_1 + m_2)$. In addition, the region near $\xi = 0$ on the real axis contributes to the energy integral in Eq. **5** when $A(\xi = 0) \neq 0$, i.e., in the presence of nonzero in-gap DOS for $\Gamma \neq 0$. Incorporating all the contributions, we obtain an expression for $D(T)$ by deforming the path of integration from the real axis to a suitably chosen contour on the complex plane that passes through the two saddle points and the region near $\xi = 0$ on the real axis (*SI Appendix*, section 6).

Thus, we get $D(T) = D_g(T) + D_0(T)$, where $D_g(T)$ is the gap-edge contribution arising from the two saddle points and $D_0(T)$ is the impurity-induced in-gap DOS. The saddle-point contribution

$$D_g(T) = \frac{1}{\pi\hbar^2}\mathrm{Re}\sum_{k,p,\zeta} M_{kp\zeta} R_T\, e^{-\pi k/\omega_c|\tau_{kp}|}\, e^{\imath 2\pi k s_{kp}(F_\zeta/B)} \qquad [9]$$

corresponds to the oscillations from energy levels passing through the gap edges $\mathcal{E}_{c/v}$ shown in Fig. 2 *C* and *D*. Here k labels the harmonics, $p = \pm$, $\zeta = \pm$. The T-dependent amplitude $R_T = (\pi\Delta_I/T)^{1/2}\exp(-\Delta_I/2T)$ has a Schottky-like activated form controlled by the indirect gap. The Dingle damping is controlled by a field, temperature, and impurity scattering-dependent $1/|\tau_{kp}|$, where $\hbar/\tau_{kp} = [2\gamma m_+/(m_1 + m_2) + pk\pi(\Delta_I T/\hbar\omega_c)]$ with $\gamma = \Gamma_1 - \Gamma_2$. The factor $M_{kp\zeta}$ is given by $M_{kp\zeta} = -\zeta(ps_{kp})^{3/2}\exp(-\imath\zeta\Gamma_c/T)(m_1 + m_2)/2$, where $s_{kp} = \mathrm{sgn}(\tau_{kp})$.

We emphasize several important features of Eq. **9**. The most significant result here is the analytical expression $F_\pm = F_0 \mp (m_2 - m_1)\Delta_I/(4\hbar e)$ for the oscillation frequencies. How these frequencies originate from the gap-edge states was discussed in *Section 2* (Fig. 2 *C* and *D*). In our analysis, they can be traced to the real part of the pole $l_p(\tilde{\xi}_{k\zeta}) = (F_\zeta/B) + \imath/(2\omega_c\tau_{kp})$ at the complex saddle point.

The two close-by frequencies $F_\pm$ give rise to a beat pattern at low T. We can see this clearly in our numerical results in Fig. 3*C*, which were obtained by numerically evaluating $D(T)$ using Eqs. **5** and **6**. We analytically show in *SI Appendix*, section 4 that F_ζ s emerge from the $1/B$-periodic crossing of energy levels $\mathcal{E}_{l\pm}$ through the gap edges $\mathcal{E}_{c/v}$ (Fig. 2 *B* and *C*). This is also demonstrated in Fig. 3*C*, where we plot the gap or the difference $\Delta_g(B) = (E_+ - E_-)$ of maximum and minimum energy eigenvalues (Eq. **2**) corresponding to the valence and conduction bands as a function of $1/B$. The beat pattern in LE-DOS oscillations at low temperature correlates with $\Delta_g(B)$.

Following ref. 26, this B-dependent gap Δ_g can be used to construct a simple model for resistivity oscillations for the disorder-free case at low temperature through the relation $\rho \sim \exp[\Delta_g(B)/T]$. This leads to similar oscillatory behavior (Fig. 3*C*) and nonmonotonic non-LK temperature dependence of oscillation amplitude (Fig. 4*A*) at low temperatures for the resistivity as in the LE-DOS.

Another important feature of Eq. **9** is the Dingle damping that arises from the imaginary part of the pole. Note the unusual T and B dependence of the Dingle factor $\sim\exp[-k\pi^2(\Delta_I T/\hbar^2\omega_c^2)]$ in the absence of impurities. This leads to a Gaussian peak in the Fourier transform (FT) spectrum of the oscillations unlike the usual Lorentzian peak.

The low-temperature beat pattern has been alluded to in ref. 22 based on numerical calculations for a model with a constant hybridization. Here, we give a controlled analytical derivation and clear physical picture (Fig. 2 *C* and *D*) of the beat frequencies and obtain the field, temperature, and disorder dependence of the associated oscillations.

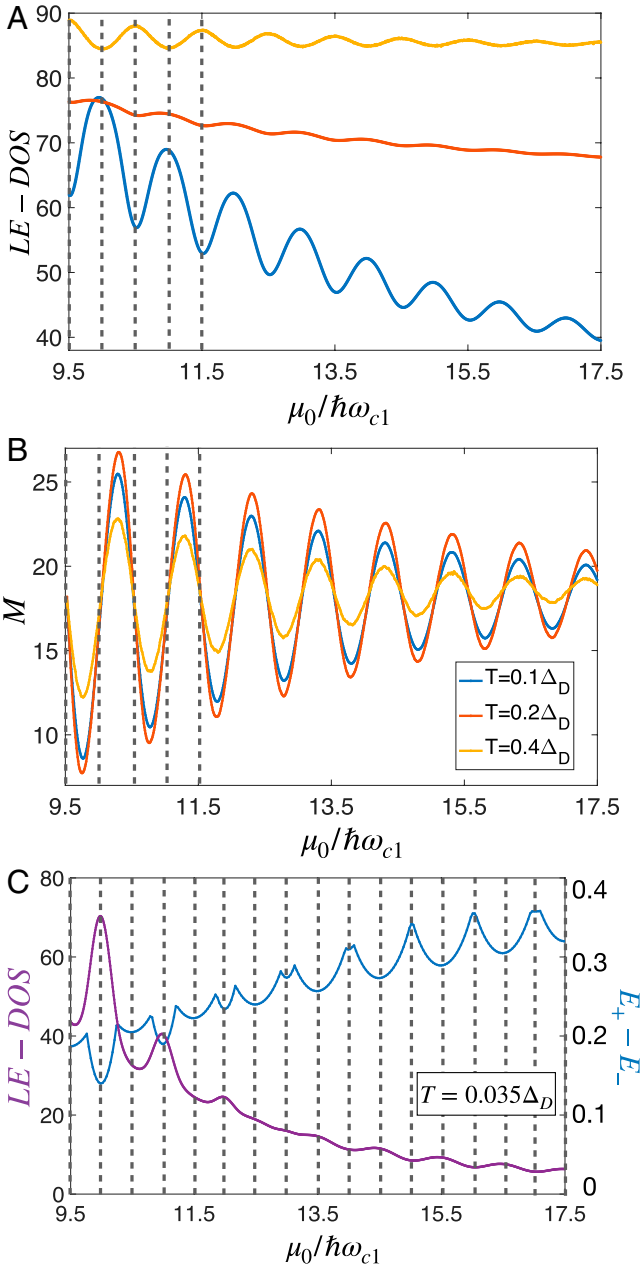

Fig. 3. LE-DOS and magnetization oscillations. (*A*) LE-DOS vs. $1/B$ for $\Gamma = 0$ and chemical potential μ_0 at three temperatures indicated in *B*. The vertical dashed lines are a guide to the eye for the π-phase shift between low- and high-temperature oscillations. The oscillation amplitude becomes very small at $T = 0.2\Delta_D$, close to $T = T_\pi$ where the π-phase shift occurs. (*B*) Magnetization oscillations for three different temperatures. The amplitude shows nonmonotonic temperature dependence. The contrast of dHvA oscillations with LE-DOS oscillations (*A*), unlike in a metal, is evident. (*C*) The beat pattern in LE-DOS oscillations at low temperature ($T = 0.035\Delta_D$) correlates with the difference $(E_+ - E_-)$ in eigenenergies closest to the gap edges $\mathcal{E}_{c/v}$ (Fig. 2 *E* and *F*). All the results in *A*–*C* are obtained using the energy eigenvalues $\mathcal{E}_{l,b\pm}$ in Eq. **2**. $E_+ - E_-$ in *C* is given in units of Δ_D.

We next turn to the impurity-induced in-gap LE-DOS, arising from the region near $\xi = 0$ in the integral of Eq. **5**, which is given by

$$D_0(T) = \frac{2}{\pi\hbar^2}\cos\left[2\pi\left(\frac{F_0}{B}\right)\right]\sum_{k,p}\tilde{M}_p\tilde{R}_{T,kp}\, e^{-\pi k/\omega_c\tilde{\tau}_p}. \qquad [10]$$

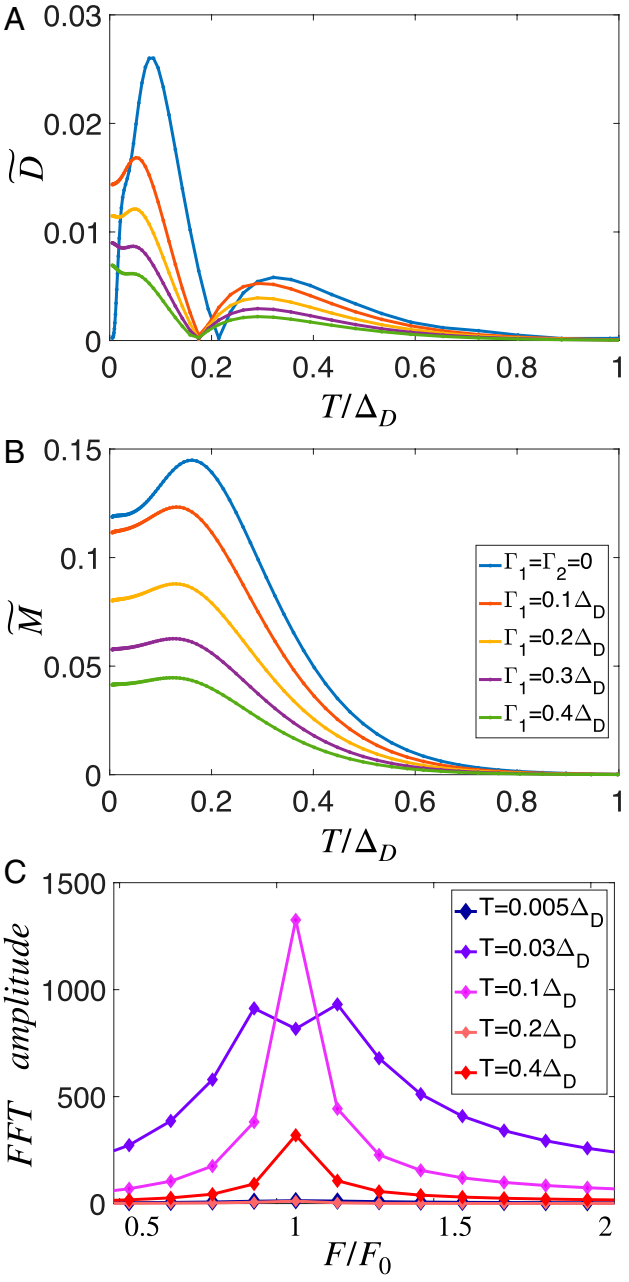

Fig. 4. Temperature dependence of LE-DOS and magnetization oscillation amplitude. (*A*) LE-DOS oscillation amplitude $\tilde{D}$ at frequency F_0 as a function of temperature for different impurity-scattering rates, as indicated in *B*. $\tilde{D}$ is extracted from the FT spectrum of LE-DOS oscillations and is normalized by the $T=0$ value of the amplitude $\tilde{D}_{v=0}(0)$ for zero hybridization. Small scattering rates $\Gamma_1=\Gamma_2=0.0005\Delta_D$ have been used for numerical computation of LE-DOS in the disorder-free case (blue line). For all finite Γ_1s, $\Gamma_2=0.1\Delta_D$. (*B*) Magnetization oscillation amplitude at F_0, $\tilde{M}(T)$, normalized by its $T=0$ value $\tilde{M}_{v=0}(0)$ for zero hybridization (see *SI Appendix*, section 9 for details). The results in *A* and *B* are obtained using the energy eigenvalues $\mathcal{E}_{l,b\pm}$ in Eq. **2**. (*C*) FT spectrum at several temperatures for the disorder-free system. The peaks at frequencies F_ζ from gap-edge oscillations are visible at $T=0.03\Delta_D$.

This result is the same as that derived in ref. 12, which, however, did not obtain $D_g(T)$. Here $\tilde{M}_p=(1/2)[(m_1+m_2)\,\Gamma_c/\sqrt{\Gamma_c^2+(\Delta_I/2)^2}+p(m_1-m_2)]$ and $\tilde{R}_{T,kp}=\chi/\sinh\chi$, with $\chi=2\pi^2\tilde{M}_pkT/\hbar eB$, is an effective LK-like T-dependent factor governed by both band masses and impurity scattering. The Dingle damping factor is $1/\tilde{\tau}_p=[\sqrt{\Gamma_c^2+(\Delta_I/2)^2}+p\Gamma_r]/\hbar$ with $\Gamma_r=(m_1\Gamma_1-m_2\Gamma_2)/(m_1+m_2)$.

The amplitudes of the LE-DOS oscillations due to gap edges (Eq. **9**) and the in-gap states (Eq. **10**) have completely different temperature dependences. The former is identically zero at $T=0$ and increases in an activated manner with T irrespective of the strength of impurity scattering. In contrast, the amplitude of oscillations from in-gap states decreases as a function of T with an effective LK form and is present only for $\Gamma\neq 0$.

Remarkably, these two contributions coexist as shown by the contour integral calculation above. This analysis, however, is valid only at low temperature $T\ll\Delta_I$. For higher temperatures, $\Delta_I\lesssim T\ll\hbar\omega_{c1}$, we complement our analytical results by numerical evaluation of Eq. **5**. The results for the LE-DOS as a function of $\mu_0/\hbar\omega_{c1}$ in the disorder-free case are shown in Fig. 3*A* for three different temperatures. We find similar features for $\Gamma\neq 0$. We also see, consistent with ref. 10, that there is a π-phase shift of the oscillations at a temperature $T_\pi\sim\Delta_I/2$, which coincides with the temperature at which the FT amplitude $\widetilde{D}$ vanishes, as shown in Fig. 4*A*. T_π shifts to a slightly lower value for nonzero Γ. The vanishing of $\widetilde{D}$ and the phase shift arise from an interference effect between oscillations with different frequencies. It is tempting to ascribe this to Berry phase effects (10) near the band edges, since the Hamiltonian of Eq. **1** has nontrivial band topology (10, 24, 27). However, we have numerically found similar interference effects even in a model with a constant hybridization that is topologically trivial.

The presence of different frequencies arising from the gap edges and from in-gap states can also be seen in our numerical FT spectrum in Fig. 4*C*. At higher temperatures $\Delta_I<T<\hbar\omega_{c1}$, the effect of the gap becomes negligible due to thermal excitations and we expect to recover standard oscillations of a metal. Thus, in our numerical FT spectrum in Fig. 4*C*, we find that two frequencies $F_0\pm\delta F$, seen at low temperature, merge into a single frequency F_0 at higher temperature.

In Fig. 4*A*, for the chosen range of values of Γ, the FT amplitude $\widetilde{D}\equiv\widetilde{D}(F_0)$ at frequency F_0 decreases with increasing impurity scattering as expected from the Dingle damping in both $D_g(T)$ (Eq. **9**) and $D_0(T)$ (Eq. **10**). However, the amplitude $\widetilde{D}(F_0)$ can have much more subtle nonmonotonic dependence on both T and Γ, for different choices of Γ, as we show in *SI Appendix*, section 7. This is because the saddle-point contribution $D_g(T)$ leads to a Gaussian peak at frequency F_ζ in the FT spectrum and affects the amplitude at the close-by frequency F_0 due to its finite width arising from the Dingle damping in Eq. **9**. As a result, LK-like temperature dependence of $D_0(T)$ and activated behavior of $D_g(T)$ both contribute to temperature dependence of $\widetilde{D}$ in general, leading to complicated nonmonotonic T dependence (*SI Appendix*, section 7).

4. Magnetization

In *Section 3*, the dHvA oscillations at $T=0$ were explained in terms of a fictitious particle–hole symmetric gapped spectrum $\tilde{\mathcal{E}}_\pm$ (Fig. 2 *E* and *F*), where the semiclassical k-space orbits at the gap edges have exactly the same area as the unhybridized crossing (Fig. 2 *A* and *B*) corresponding to the frequency F_0. Here we confirm that the oscillations with frequency F_0 persist at finite temperature and obtain an analytical expression for the oscillatory part of M for $T\ll\Delta_I,\hbar\omega_c$ via a saddle-point approximation. We show that the saddle point for M is completely different from the one that contributes to LE-DOS gap-edge oscillations and thus affirm the unusual dichotomy between dHvA and SdH oscillations in hybridization-gap insulators. We corroborate our

analytical approximations through numerical calculations that extend to higher temperature.

To compute the magnetization, we use the Matsubara representation of the grand potential (9, 28) $\Omega(T) = -TN_B[\sum_{\omega_n>0,l,bp} \ln(\mathcal{E}_{l,bp} - \mu_0 - \imath\omega_n)e^{\imath\omega_n 0^+} + \text{c.c.}]$, where $\omega_n = (2n+1)\pi T (n \in \mathbb{Z})$ are fermionic frequencies (*SI Appendix*, section 8.B). In the semiclassical limit $\mu_0 \gg \hbar\omega_{c1}$ we can write the oscillatory part of magnetization $M(T) = -\partial\Omega(T)/\partial B$ as

$$M = \frac{8\pi T\mu_0}{\hbar\omega_{c1}\phi_0} \sum_{p,k=1}^{\infty} \left[\sum_{n=0}^{\infty} F_{kp}(n)\right]. \qquad [11]$$

Here $F_{kp}(n) \equiv F_{kp}(\imath\omega_n)$ is given by the expression $F_{kp}(n) = \sin[2\pi k(F_0/B)]e^{2\pi\imath k s_p(n)\text{Im}[l_p(n)]}$. $l_p(n)$ denotes the pole $l_p(\xi)$ in Eq. **7** with $\xi \to \imath\omega_n$ (*SI Appendix*, sections 5 and 8.B) and $s_p(n) = \text{sgn}[\text{Im}\{l_p(n)\}]$.

As shown in *SI Appendix*, section 8.C, we evaluate the Matsubara sum in Eq. **11** for $T \ll \Delta_I, \hbar\omega_c$ using the Euler–Maclaurin formula

$$T\sum_{n=0}^{\infty} F_{kp}(n) \approx \int_0^{\infty} \frac{d\omega}{2\pi} F_{kp}(\imath\omega) + \frac{T}{2}[F_{kp}(0) + F_{kp}(\infty)], \qquad [12]$$

where we have used $dn = d\omega/(2\pi T)$ and $F_{kp}(n\to\infty) = 0$. The integral in the first term does not depend on temperature and can be evaluated using a saddle-point approximation. The saddle point $\tilde{\omega} = (-\Gamma_c - m_r\Delta_I/2\sqrt{1-m_r^2})$, with $m_r = (m_2 - m_1)/(m_1 + m_2)$, is different from the saddle points that govern the LE-DOS integral (Eq. **5**). The saddle point here leads to the pole at $l_p(\tilde{\omega}) = (F_0/B) + \imath/(2\omega_c\tau_p)$ with $1/\tau_p = [2m_+\gamma/(m_1+m_2) + (p+m_r^2)\Delta_I/(2\sqrt{1-m_r^2})]/\hbar$. The real part of the pole gives rise to an oscillation frequency F_0, as if the system has a Fermi surface with an area πk_F^2 like a metal. But, unlike a metal, here the frequency appears from the underlying fictitious particle–hole symmetric gapped system of Fig. 2 *E* and *F*.

The temperature dependence in $M(T)$ comes from the next order terms in Eq. **12**. Keeping only the leading correction in $T/\sqrt{\hbar\omega_c\Delta_I}$, we obtain

$$M \propto \sin\left[2\pi k\left(\frac{F_0}{B}\right)\right] \sum_{p,k=1}^{\infty} \left[\frac{(1-m_r^2)^{3/2}}{\sqrt{k}} e^{-\pi k/\omega_c|\tau_p|} + \frac{\pi T}{\sqrt{\hbar\omega_c\Delta_I}} e^{-\pi k/\omega_c\tau_{1p}(T)} + \dots\right]. \qquad [13]$$

Here we have assumed $\Delta_I > \gamma$ to simplify the expression (*SI Appendix*, section 8.C). This result implies a Dingle damping $\exp(-\pi\Delta_I/2\hbar\omega_c)$ for the clean system ($\Gamma = 0$).

In Eq. **13**, $\tau_{1p}(T) = [((\pi T + \Gamma_c)^2 + (\Delta_I/2)^2)^{1/2} + p(\Gamma_r - m_r\pi T)]$ is a temperature-dependent damping factor. This suggests the existence of a peak in the amplitude of one of the oscillation components ($p=+$) at a temperature $T_{\text{peak}} \simeq [m_r\Delta_I/(2\sqrt{1-m_r^2}) - \Gamma_c]/\pi$, which shifts toward lower temperature with increasing impurity-scattering Γ_c. The peak eventually goes away when $\Gamma_c \gtrsim \Delta_I$, as one anticipates the impurity-induced DOS to fill up the gap completely in this limit. We note that the low-temperature expansion in Eq. **13** is not strictly valid at $T \sim T_{\text{peak}} \sim \Delta_I$; however, we expect it to reproduce the qualitative features even at intermediate temperatures. Our numerical results confirm this expectation as we discuss below. The low-T expression of Eq. **13** leads to non-LK temperature dependence of dHvA oscillations in the hybridized insulator.

For our numerical calculations in the disorder-free case $\Gamma = 0$, we compute $M(T)$ using

$$\Omega(T) = -\int_{-\infty}^{\infty} d\xi \frac{\partial n_F(\xi, T)}{\partial\xi} \Omega(\xi, T=0), \qquad [14]$$

for the grand potential at finite temperature with chemical potential μ_0. Here $\Omega(\xi, T=0) = N_B \sum'_{lbp}(\mathcal{E}_{l,bp} - \mu_0 - \xi)$ is the grand potential or total energy at $T=0$, where the sum is restricted to $\mathcal{E}_{lbp} \le \mu_0 + \xi$ (*SI Appendix*, section 9). The numerical results for the magnetization oscillations obtained using the energy eigenvalues of Eq. **2** with $\Gamma = 0$ are shown in Fig. 3*B* as a function of $1/B$ for three temperatures. The oscillation frequency is indeed F_0, in agreement with our analytical results in the semiclassical limit. The FT amplitude $\widetilde{M} \equiv \widetilde{M}(F_0)$ at frequency F_0 is shown in Fig. 4*B*; $\widetilde{M}$ exhibits nonmonotonic behavior with T with a peak at intermediate temperature, as predicted by the low-T expansion in Eq. **13**.

To obtain the magnetization oscillations in a disordered system with $\Gamma \neq 0$, we use a semiclassical expression similar to Eq. **11**, albeit generalized to incorporate the actual energy eigenvalues (Eq. **2**), as discussed in *SI Appendix*, section 9. Again, we find M oscillations with unhybridized frequency F_0. The FT amplitude $\widetilde{M}$ is shown as a function of temperature for several Γ_1 for fixed $\Gamma_2 \le \Gamma_1$ in Fig. 4*B*. The amplitude shows a peak at intermediate temperature, like the $\Gamma = 0$ case; however, the peak gets weaker with increasing Γ, in qualitative agreement with the analytical result (Eq. **13**). We find qualitatively the same result for $\Gamma_1 < \Gamma_2$, as shown in *SI Appendix*, Fig. S3 in *SI Appendix*, section 9.

5. Discussion and Conclusions

We have focused in this paper on a minimal model of a hybridization-gap insulator and our results are summarized in Table 1. The physical picture explaining the origin of SdH and dHvA oscillations, and why they differ qualitatively, is summarized in Fig. 2. In this section, we conclude with a discussion of the assumptions underlying our model, the universality of our main results, and their possible relation to experiments.

Our results are obtained in an insulating regime when the chemical potential lies in the gap. The insulating nature of the state requires that certain conditions be met. First, we need $B < B_c = \sqrt{m_1 m_2}\Delta_D/\hbar e$, the critical field above which the system undergoes an insulator-to-metal transition even in the absence of disorder (Fig. 1*B*). Second, when we include the effects of impurities, we must ensure that they do not drive the system metallic.

The role of impurities in an insulator where a heavy inverted band hybridizes with a light band has been analyzed in detail in ref. 29. The nature of the impurity-bound state wavefunction in such a band structure differs qualitatively from that in ordinary semiconductors and results in a localized "impurity band." However, the long-range Coulomb interactions that lead to this behavior are hard to include in the analysis of quantum oscillations. Thus, we treat impurity effects following ref. 12 as self-energies that arise in an approximation akin to the coherent potential approximation (CPA).

We focus on the regime of weak disorder broadening $|\Gamma_1 - \Gamma_2| < \Delta_D$, the direct band gap, or else the system enters a semimetallic regime (12) as deduced from the real part of the energy eigenvalues of the non-Hermitian Hamiltonian. To check the insulating nature of the weak disorder regime, we have computed the direct current (DC) conductivity at $B = 0$ using the Kubo formula within an approximation that includes impurity self-energies in Green's functions but ignores vertex corrections (*SI Appendix*, section 10). We find that there is an insulating upturn in the DC resistivity ($d\rho/dT < 0$), which nevertheless has a large but finite value at $T = 0$ in the disordered system. In the absence of impurities, we would of course get an activated resistivity that diverges at $T = 0$.

Our results are based on an insulating gap arising from the hybridization of two bands, although we focused on odd-parity hybridization that is not essential for our analysis. An important question is the extent to which our results give insight into systems where the insulating gap results from interaction as in the Kondo insulators (3–5, 30) or excitonic insulators, which may be relevant for the semiconductor superlattices (7, 8).

We note that, within a mean-field theory (MFT) of both these systems, one simply obtains an effective two-band model like the one we analyze. The analog of the direct gap Δ_D in our model is determined by the exciton condensate order parameter in the MFT (31–34) for exciton insulators. Similarly, Δ_D is determined by the hybridization amplitude in the slave-boson MFT of Kondo insulators (35, 36). One important difference with our model is that the mean-field order parameters, and thus the resulting hybridization, may have nontrivial B dependence, as noted in ref. 34. However, these authors show that these effects are expected to influence only the higher harmonics of the quantum oscillations and not to modify the characteristic features of fundamental harmonics, which is our main focus.

Finally, we turn to insulating systems—semiconductor quantum wells and Kondo insulators—where quantum oscillations are well established, even though the experiments are often seemingly inconsistent with each other. We do not discuss quantum oscillations (37) in insulating monolayer WTe_2 since their intrinsic nature is under debate (38).

In semiconductor quantum wells, the band structure is not "rigid" and is expected to change significantly due to changes in screening when the system is gated from a metallic to an insulating regime. The two InAs/GaSb experiments of refs. 7 and 8 find an order of magnitude difference in the observed SdH frequencies in the insulating regime. This large difference in frequencies could be the result of different band structure renormalizations in the two samples, which is beyond the scope of our theory. Given an appropriate insulating band structure, however, a model similar to ours should be applicable once μ lies within the gap. Importantly, we note that the SdH amplitudes in the two InAs/GaSb experiments see qualitatively different T dependences. A monotonically decreasing LK-like T dependence is observed in ref. 8 (Fig. 2*A*), whereas a monotonical increase is seen in ref. 7 (Fig. 3*C*). According to our theory, the LK-like behavior in ref. 8 suggests dominance of impurity-induced in-gap DOS oscillations in the system, whereas increase of the amplitude with temperature in ref. 7 points toward the role of gap-edge oscillations. Thus, these experimental observations imply that the consideration of both gap-edge and in-gap contributions to SdH oscillations, emphasized in our work, is crucial for a proper understanding of the T dependence of SdH oscillations when impurity effects can widely vary from one system to another.

The beat pattern from gap-edge oscillations at frequencies $F_0 \pm \delta F$ has not yet been reported in SdH experiments. We emphasize that the resolution of the beat frequencies might be difficult in practice due to three close-by frequencies in a narrow band-gap insulator with field damping and impurity scattering and due to the limited range of the low-temperature regime where the beats are expected to exist (Fig. 4*C*). As shown in Fig. 4*A* and *SI Appendix*, Fig. S2 (*SI Appendix*, section 7), the existence of the three close-by frequencies, even when they cannot be clearly resolved, leads to complex temperature dependence of the SdH amplitude depending on the disorder strength. Such anomalous T dependence might be easier to observe and analyze in experiments than to resolve the beat frequencies directly.

Quantum oscillations have been seen in two Kondo insulators SmB_6 and YbB_{12}. In SmB_6, the data of refs. 3, 30, and 39 show bulk dHvA oscillations with an amplitude exhibiting a remarkable increase over the LK form at the lowest temperatures. Other experiments (2, 40), however, do not see bulk oscillations in SmB_6 and report dHvA oscillations only from the sample surface, which is perhaps not surprising in a topological Kondo insulator with protected surface states. The unusual temperature dependence of the dHvA oscillation amplitude of refs. 3 and 30 is not captured within the model we have analyzed nor in any other theory that we are aware of. Also, this non-LK T dependence is not seen in other Kondo insulators like YbB_{12} as we discuss below.

Although SdH oscillations in transport have not been reported in SmB_6, very recently, quantum oscillations have been observed in specific heat (41), although the T dependence of the amplitude has not been studied. We expect specific heat oscillations to be qualitatively similar to those in the LE-DOS, effectively controlled by the lowest-energy excitations to the gap edges and disorder-induced in-gap states as in the semiclassical picture of Fig. 2 *C* and *D*.

Quantum oscillations with an LK-like T dependence have been reported in YbB_{12} by two groups (4, 5), but there are significant differences in their observed frequencies and their 3D/2D nature. Ref. 5 reports bulk dHvA oscillations. Ref. 4 reports both dHvA and SdH oscillations, ascribing their SdH data to the bulk, but it is not clear whether the dHvA data arise from the surface or the bulk (42, 43). An additional complication in YbB_{12} is the field-induced transitions in the insulating state (42) that make it hard to analyze quantum oscillations over a sufficiently broad field range.

Within the noninteracting model of a hybridization-gap insulator discussed in this paper, the observation of LK-like behavior implies a dominant role of impurity-induced in-gap states. However, interaction effects beyond the noninteracting model (35, 36) may play a vital role in the strongly correlated insulators like SmB_6 and YbB_{12}.

Even though none of the existing theories can make quantitative connections with the observed quantum oscillations, we emphasize that any theory of such oscillations in an insulator where the gap results from an effective hybridization will necessarily have to build on the theory of quantum oscillations that is developed here. Our analytical results will serve as a template to incorporate more subtle and exotic effects of interactions, at the very least through frequency-dependent self-energies, in strongly correlated Kondo insulators. The features that we have unearthed through our analytical semiclassical results, and for which we provide a simple physical picture, are universal insofar as the dichotomy between dHvA and SdH oscillation frequencies, the nature of the field and temperature dependence of the amplitudes, and the role of disorder in giving an in-gap contribution that adds to the gap-edge oscillations in the low-energy DOS.

Materials and Methods

The details of the analytical calculations presented in the main text are described in *SI Appendix*. We also describe some details of our numerical calculations and present additional numerical results (44). In *SI Appendix*, Table S1 we define symbols used in the main text. We then discuss how one takes the semiclassical limit of our model and analytically compute the frequency of the gap-edge oscillations and the field at which an insulator-to-metal transition occurs. We then discuss in detail the saddle-point analysis for the LE-DOS oscillations, both in the clean case and with the inclusion of disorder. Next, we describe in detail the analytical and numerical calculations for the magnetization oscillations. We conclude with a brief discussion of transport in the disordered insulator.

Data, Materials, and Software Availability. Data files for figures and matlab source codes have been deposited in https://zenodo.org/badge/latestdoi/521568110 (10.5281/zenodo.6967367) (44).

All other data are included in the article and/or supporting information.

ACKNOWLEDGMENTS. We thank Lu Li, Yuji Matsuda, Nitin Samarth, Suchitra Sebastian, and Brian Skinner for useful discussions. S.B. acknowledges support from Science and Engineering Research Board (SERB) (ECR/2018/001742), Department of Science and Technology (DST), India and the American Physical Society's International Research Travel Award Program. M.R. was supported by NSF Materials Research Science and Engineering Center Grant DMR-2011876.

1. D. Shoenberg, *Magnetic Oscillations in Metals* (Cambridge Monographs on Physics, Cambridge University Press, 1984).
2. G. Li *et al.*, Two-dimensional fermi surfaces in kondo insulator SmB_6. *Science* **346**, 1208 (2014).
3. B. S. Tan *et al.*, Heavy fermions. Unconventional Fermi surface in an insulating state. *Science* **349**, 287–290 (2015).
4. Z. Xiang *et al.*, Quantum oscillations of electrical resistivity in an insulator. *Science* **362**, 65–69 (2018).
5. H. Liu *et al.*, Fermi surfaces in Kondo insulators. *J. Phys. Condens. Matter* **30**, 16LT01 (2018).
6. N. P. Ong, Quantum oscillations in an insulator. *Science* **362**, 32–33 (2018).
7. Z. Han, T. Li, L. Zhang, G. Sullivan, R. R. Du, Anomalous conductance oscillations in the hybridization gap of $InAs/GaSb$quantum wells. *Phys. Rev. Lett.* **123**, 126803 (2019).
8. D. Xiao, C. X. Liu, N. Samarth, L. H. Hu, Anomalous quantum oscillations of interacting electron-hole gases in inverted type-ii $InAs/GaSb$quantum wells. *Phys. Rev. Lett.* **122**, 186802 (2019).
9. J. Knolle, N. R. Cooper, Quantum oscillations without a fermi surface and the anomalous de Haas–van Alphen effect. *Phys. Rev. Lett.* **115**, 146401 (2015).
10. L. Zhang, X.-Y. Song, F. Wang, Quantum oscillation in narrow-gap topological insulators. *Phys. Rev. Lett.* **116**, 046404 (2016).
11. J. Knolle, N. R. Cooper, Anomalous de haas–van Alphen effect in $InAs/GaSb$quantum wells. *Phys. Rev. Lett.* **118**, 176801 (2017).
12. H. Shen, L. Fu, Quantum oscillation from in-gap states and a non-Hermitian Landau level problem. *Phys. Rev. Lett.* **121**, 026403 (2018).
13. G. Baskaran, Majorana fermi sea in insulating SmB6: A proposal and a theory of quantum oscillations in Kondo insulators. arXiv [Preprint] (2015). https://doi.org/10.48550/arXiv.1507.03477 (Accessed 13 July 2015).
14. O. Erten, P.-Y. Chang, P. Coleman, A. M. Tsvelik, Skyrme insulators: Insulators at the brink of superconductivity. *Phys. Rev. Lett.* **119**, 057603 (2017).
15. I. Sodemann, D. Chowdhury, T. Senthil, Quantum oscillations in insulators with neutral fermi surfaces. *Phys. Rev. B* **97**, 045152 (2018).
16. D. Chowdhury, I. Sodemann, T. Senthil, Mixed-valence insulators with neutral Fermi surfaces. *Nat. Commun.* **9**, 1766 (2018).
17. C. M. Varma, Majoranas in mixed-valence insulators. *Phys. Rev. B* **102**, 155145 (2020).
18. J. Knolle, N. R. Cooper, Excitons in topological kondo insulators: Theory of thermodynamic and transport anomalies in SmB_6. *Phys. Rev. Lett.* **118**, 096604 (2017).
19. P. Ram, B. Kumar, Theory of quantum oscillations of magnetization in Kondo insulators. *Phys. Rev. B* **96**, 075115 (2017).
20. H. K. Pal, F. Piéchon, J.-N. Fuchs, M. Goerbig, G. Montambaux, Chemical potential asymmetry and quantum oscillations in insulators. *Phys. Rev. B* **94**, 125140 (2016).
21. H. K. Pal, Quantum oscillations from inside the fermi sea. *Phys. Rev. B* **95**, 085111 (2017).
22. H. K. Pal, Unusual frequency of quantum oscillations in strongly particle-hole asymmetric insulators. *Phys. Rev. B* **96**, 235121 (2017).
23. S. Grubinskas, L. Fritz, Modification of the Lifshitz-Kosevich formula for anomalous de Haas–van Alphen oscillations in inverted insulators. *Phys. Rev. B* **97**, 115202 (2018).
24. R. Peters, T. Yoshida, N. Kawakami, Quantum oscillations in strongly correlated topological kondo insulators. *Phys. Rev. B* **100**, 085124 (2019).
25. W.-Y. He, P. A. Lee, Quantum oscillation of thermally activated conductivity in a monolayer WTe_2-like excitonic insulator. *Phys. Rev. B* **104**, L041110 (2021).
26. P. A. Lee, Quantum oscillations in the activated conductivity in excitonic insulators: Possible application to monolayer WTe_2. *Phys. Rev. B* **103**, L041101 (2021).
27. V. Alexandrov, P. Coleman, O. Erten, Kondo breakdown in topological Kondo insulators. *Phys. Rev. Lett.* **114**, 177202 (2015).
28. S. A. Hartnoll, D. M. Hofman, Generalized Lifshitz-Kosevich scaling at quantum criticality from the holographic correspondence. *Phys. Rev. B Condens. Matter Mater. Phys.* **81**, 155125 (2010).
29. B. Skinner, Properties of the donor impurity band in mixed valence insulators. *Phys. Rev. Mater.* **3**, 104601 (2019).
30. M. Hartstein *et al.*, Fermi surface in the absence of a Fermi liquid in the Kondo insulator SmB_6. *Nat. Phys.* **14**, 166 (2018).
31. J. Cloizeaux, Exciton instability and crystallographic anomalies in semiconductors. *J. Phys. Chem. Solids* **26**, 259 (1965).
32. D. Jérome, T. M. Rice, W. Kohn, Excitonic insulator. *Phys. Rev.* **158**, 462 (1967).
33. B. I. Halperin, T. M. Rice, Possible anomalies at a semimetal-semiconductor transition. *Rev. Mod. Phys.* **40**, 755 (1968).
34. A. A. Allocca, N. R. Cooper. Quantum oscillations in interaction-driven insulators. *SciPost Phys.* **12**, 123 (2022).
35. A. C. Hewson, *The Kondo Problem to Heavy Fermions* (Cambridge Studies in Magnetism , Cambridge University Press, 1993).
36. P. Coleman, *Introduction to Many-Body Physics* (Cambridge University Press, 2015).
37. P. Wang *et al.*, Landau quantization and highly mobile fermions in an insulator. *Nature* **589**, 225–229 (2021).
38. J. Zhu *et al.*, Quantum oscillations in two-dimensional insulators induced by graphite gates. *Phys. Rev. Lett.* **127**, 247702 (2021).
39. M. Hartstein *et al.*, Intrinsic bulk quantum oscillations in a bulk unconventional insulator SmB_6. *iScience* **23**, 101632 (2020).
40. Z. Xiang *et al.*, Bulk rotational symmetry breaking in kondo insulator SmB_6. *Phys. Rev. X* **7**, 031054 (2017).
41. P. G. LaBarre *et al.*, Magnetoquantum oscillations in the specific heat of a topological kondo insulator. arXiv [Preprint] (2022). https://doi.org/10.1088/1361-648X/ac7d2b. (Accessed 11 April 2022).
42. Z. Xiang *et al.*, Hall anomaly, quantum oscillations and possible Lifshitz transitions in kondo insulator YbB_{12}: Evidence for unconventional charge transport. *Phys. Rev. X* **12**, 021050 (2022).
43. Z. Xiang *et al.*, Unusual high-field metal in a kondo insulator. *Nat. Phys.* **17**, 788 (2021).
44. A. Panda, S. Banerjee, M. Randeria, animeshphy/QOsc_in_insulators: Quantum oscillation in the Magnetization and Density of States of insulators. Zenodo. https://zenodo.org/record/6967367. Deposited 5 August 2022.